An Erosion Aggressiveness Index (EAI) based on Pressure Load Estimation due to Bubble Collapse in Cavitating Flows within the RANS Solvers

Bergeles G. [1], Li J.[2], Wang L.[2], Koukouvinis P.[1] and Gavaises M. [1]

[1]Department of Engineering and Mathematical Sciences, City University, Northampton Square, London, EC1V0HB, UK
[2]Caterpillar Inc., Peoria, Illinois Area US, 61602US.

Abstract

Despite numerous research efforts, there is no reliable and widely accepted tool for the prediction of erosion prone material surfaces due to collapse of cavitation bubbles. In the present paper an Erosion Aggressiveness Index (EAI) is proposed, based on the pressure loads which develop on the material surface and the material yield stress. EAI depends on parameters of the liquid quality and includes the fourth power of the maximum bubble radius and the bubble size number density distribution. Both the newly proposed EAI and the Cavitation Aggressiveness Index (CAI), which has been previously proposed by the authors based on the total derivative of pressure at locations of bubble collapse ($DP/Dt>0$, $D\alpha/Dt<0$), are computed for a cavitating flow orifice, for which experimental and numerical results on material erosion have been published. The predicted surface area prone to cavitation damage, as shown by the CAI and EAI indexes, is correlated with the experiments. EAI predictions indicate the minimum bubble size above which erosion starts as also its location along the injector wall. The proposed methodology is also tested in an actual Diesel injector, operating under realistic injection cycles and pressure levels for which erosion data are available.

Introduction

Erosion of material surfaces in flow machines and hydraulic equipment due to cavitation is a fluid mechanics phenomenon which has been the focus of investigation in recent years. Hydrodynamic cavitation is the appearance of vapour within a liquid flow due to the decrease of the local pressure below the vapour saturation pressure at the local temperature [1]. Cavitation appears in various forms and it is represented by the agglomeration of bubbles containing inert gas and vapour. These bubbles are entrained to the flow and transported to regions of higher pressure where they collapse; during the collapsing phase pressure pulses are emitted to the environment and impinge either on material surfaces or on other surrounding vapour bubbles. In the first case and depending on the amplitude of the pressure waves, erosion can take place on material surfaces [2]; in the latter case the pressure waves can initiate the collapse of the surrounding bubbles resulting in a cumulative increase of the pressure wave effect [2]. Erosion damage in marine propellers and rudders due to cavitation has been identified very early in the shipping industry; cavitation with its adverse effects is finally proven to be present in a variety of fluid mechanics processes, as fuel injectors [2], hydraulic pumps and turbines [2] and even mechanical heart valves [2]. Apart from the erosion of material surfaces the bubble collapse causes among others, machinery vibrations, noise and loss of machinery efficiency. The ability to quantify erosion prone surfaces due to hydrodynamic cavitation is an open scientific problem today.

The collapse of a bubble (containing inert gas and vapour) due to the sudden increase of the environmental pressure can be calculated from the solution of the Rayleigh-Plesset equation, and the emitted acoustic pressure pulse during the phase of bubble collapse is given by equation (1), Brennen [1]:

$$P_{ac} = \frac{\rho_l}{4\pi r}\frac{d^2V}{dt^2} \qquad (1)$$

where V is the bubble volume and r the bubble distance from the wall and ρ_l the liquid density; the acoustic pressure pulse P_{ac} exhibits a *1/r* law of pressure pulse attenuation, which renders the distance from the wall of the collapsing bubble of primary importance. According to flow analysis of a collapsing bubble based on the solution of the Rayleigh-Plesset equation, the amplitude of the emitted pressure waves, as calculated using equation (1), can be as high as 100 MPa, Franc and Michel [2]. Such pressures despite the short duration of time in which they develop (typical time scale is of 1μs) are high enough to create erosion damage on the material surface if there is a cumulative effect due to synchronous bubble collapse. Iwai et al. [3] conducted experiments on the erosion characteristics of various materials due to cavitation using a vibratory facility; they measured the impact loads attributed to the collapse of vapour bubbles and were able to correlate erosion material loss with impact loads. In particular they confirmed that there exists an impact threshold value after which the bubble collapse contributes to the fatigue fracture of the material surface; the cavitation erosion loss of mass is proportional to the energy acting on the surface to a power experimentally defined. Fortes-Patella et al. [4] concluded that the damage of the material due to cavitation phenomena can be related to the characteristics of pressure waves emitted by the collapse of vapour structures; they were able to show experimentally and computationally that the pressure wave power density (which is proportional to the square of the maximum pressure pulse upon bubble collapse) is well correlated to the pit volume created on the material surface due to its elastic-plastic deformation; the previous point was proved by coupling the pressure waves load on the material surface (an output of the numerical solution of a Rayleigh-Plesset equation) with a numerical fluid-structure interaction analysis of the elastic-plastic deformation of the material surface, demonstrating that the pressure wave power density and the generated pit volume are linearly correlated. Dular et al. [5] investigated experimentally a cavitating flow around a hydrofoil in a water tunnel for various operating conditions and cavitation numbers; they visually observed the strong correlation of cavitation and erosion damage. These experiments suggested that erosion damage is well correlated with the cavitation unsteadiness and vapour cloud separation and collapse; the cloud collapse initiates a shock wave that upon impinging on the bubbles near the solid surface force them into oscillation and due to the presence of the solid wall they start an asynchronous bubble collapse. According to Plesset and Chapman [6], as a result of the asynchronous bubble collapse, a micro jet is formed towards the wall surface with an impulse which, if above a threshold value, is capable of creating plastic deformation on the material surface. They proposed an erosion model based on the correlation of the standard deviation of the deformation effects the micro jet has on the material surface, which was measured experimentally, with the emitted pressure wave. Dular and Coutier-Delgosha [7] investigated the possibility of predicting cavitation erosion in hydrofoil flows using Computational Fluid Dynamics (CFD); the CFD model was based on the numerical solution of the unsteady RANS equations coupled with a homogeneous equilibrium barotropic model. As erosion model they employed the model of Dular et al.[5]. They assumed that the micro jet is responsible for the plastic deformation of the material and the creation of pits on the solid surface, as Plesset and Chapman [6]. Li Ziru [8] investigated various erosion criteria within the concept of RANS equation on a post processing basis; she examined the predictability of the instantaneous static pressure, time derivative of pressure, time derivative of vapour volume fraction and time integrals of the previous indicators and others; she concluded that among the tested erosion indexes the time derivative of pressure seems to perform best, whilst the time derivative of the vapour volume fraction seems not to be correlated to the erosion regions. Bergeles et al. [9] proposed a Cavitation Aggressiveness Index (CAI) based on the concept of the total derivative of pressure in the flow regions of vapour collapse within the framework of RANS methodology; the regions of bubble collapse were identified as those regions of negative total derivative of the vapour volume fraction (α) (in a single fluid concept-homogeneous mixture of liquid and vapour), equation (2);

$$\frac{DP}{Dt} > 0, \frac{D\alpha}{Dt} < 0 \qquad (2)$$

The cavitation aggressiveness index (CAI) was defined as a non dimensional expression of the total derivative of pressure comparing its value to the emitted pressure pulses either due to bubble collapse or to cavity oscillations using typical corresponding time scales. The proposed index identified successfully the regions prone to erosion as reported in the measurements of Franc et al.[10]; the proposed model was also tested in another industrial case by Koukouvinis et al. [11] with success. Kato et al.[12] were among the first to propose an analytic model to compute material erosion due to cavitation; their model was based in estimating the impact force due to bubble collapse and the frequency of bubble collapses on the material surface. The number density distribution of the bubble size was taken into account in calculating the cumulative impact force due to synchronous bubble collapse; the authors pointed out the importance of the number density distribution on predicting erosion. The method successfully predicted erosion rates in cavitating hydrofoils, however it requires information not readily available, unless 'reasonable' estimations are made. Perkovic et al. [13] applied a commercially available software in predicting the flow development and the erosion rates of an injector type flow for which experimental data were available. The mathematical model was based on an incompressible, turbulent two phase flow simulation; they were able to predict the erosion velocity due to cavitation under various experimental operating conditions in the fuel injector and various fuels; the erosion model used was that employed by the commercial CFD code. Hattori et al. [14] conducted erosion tests on material surfaces due to cavitation of impacting liquid jets on the surface. The collapsing bubbles on the surface were creating impact loads which were measured with piezoelectric sensors. They found that the impact load raised to a power (which is material dependent with values from 1.1 to 1.79) multiplied with the frequency of occurrence of pressure impacts is well correlated to erosion rate of the material surface. Recently, more sophisticated models have been employed for the prediction of cavitation erosion. For example, Skoda et al [16] investigated a cavitating flow in square sectioned throttle geometry, similar to the one of the present investigation; a 2D density-based compressible Euler CFD code was used which could capture the pressure peaks created due to shock waves from the imploding bubbles. They proposed an Erosion Probability Indicator related to the maximum pressure peak on the wall and thus they were able to predict qualitatively the surface region prone to erosion. Edelbauer et al [17] investigated a similar to [16] cavitating flow and employed an LES approach for the numerical solution of the flow; they applied an erosion model which qualitatively predicted the material surface region to be eroded; the highest erosion damage was found around the tail of the vapour cloud.

In the following the proposed concept of the Erosion Aggressiveness Index (EAI) is derived and its reliability is tested in predicting two cavitating flows of engineering importance for which some data on the flow development and on erosion rates have been published.

The Erosion Aggressiveness Index (EAI)

Erosion damage due to cavitation is a time evolving process of the material damage due to pressure waves, impinging on the material surface. Various theories have been proposed for explaining material erosion and which correlate the amplitude of the pressure signature on the wall with the material properties in the elasticity and fracture regions. Vapour bubbles increase in size when moving in low pressure regions and obtain their maximum radius R_{max} at the region of lowest pressure, which usually is taken as equal to the vapour saturation pressure at the liquid temperature; as they are convected by the flow at pressure recovery regions and under the pressure difference ΔP between the surrounding pressure and the bubble pressure (P_l-P_v) the collapse phase is initiated. The emitted pressure pulse at a distance r from the bubble centre, following equation (1), is given by equation (3):

$$P_{ac} = \frac{\rho_l}{r}\frac{d}{dt}(R^2 \dot{R}) \qquad (3)$$

where R is the bubble radius and $\dot{R}$ is the velocity of the bubble wall. A mean velocity of the bubble wall during collapse, which is valid at the last stages of bubble collapse with small amount of non-condensable gas in the bubble, is given by equation (4), [1] and [2],

$$\dot{R} = \sqrt{\frac{2}{3}\frac{\Delta p}{\rho_l}}\left(\frac{R_{\max}}{R}\right)^{3/2} \qquad (4)$$

R_{max} is the maximum bubble radius at the region of minimum pressure, which is given by equation (5), assuming an isothermal expansion (Brennen [1]):

$$R_{\max} = \left(P_{g0}\frac{R_0^3}{2\sigma}\right)^{1/2} \qquad (5)$$

Expression (4) introduced into equation (3) and after some algebra leads to an approximate expression for the emitted pulse pressure in shock waves during the collapse phase and at a distance r from the bubble centre, equation (6)

$$P_{ac} = \frac{\Delta P}{3r}R_{\max}\left(\frac{R_{\max}}{R}\right)^2 \qquad (6)$$

This expression is in agreement with the estimation of the magnitude of pressure pulses emitted from a collapsing bubble, Brennen (1995, equation 3.2) [1] for a value of $\frac{R_{\max}}{R}$ =10. The emitted pressure impulse due to bubble collapse is evaluated from equation (7),

$$P_{w,imp} = P_{ac}t_b \qquad (7)$$

where t_b is the Rayleigh bubble collapsing time.

The mean impact load on the wall surface due to synchronous bubble collapse inside a volume V_{vol} can be evaluated from equation (8);

$$P_w = \iiint_{V_{vol}} P_{ac}t_b cos\varphi[-n_0\frac{D\alpha}{Dt}]dV \qquad (8)$$

where the quantity in brackets expresses in an approximate way the number of bubbles which collapse per unit time and volume; φ is the surface inclination of the wall to the radius (rad) connecting the bubble centre and the centre of the wall surface; the integration volume is a cylinder sitting on the surface with radius and height equal to L_v. Substituting expression (6) for P_{ac} and the expression of t_b (equation (11)) in equation (8) the following expression for the impact pressure (using the middle value theorem) is obtained,

$$P_w = 0.4\sqrt{\rho_l \Delta P}R_{max}^2 {L_v}^2\left(\frac{R_{max}}{R}\right)^2\overline{[-n_0\frac{D\alpha}{Dt}]} \qquad (9)$$

where n_0 is the number of bubbles per unit volume and R is the local bubble radius obtained from the volume fraction. The constant 0.4 in equation (9) is an approximate value considering also the wave attenuation due to local absorption. In the results presented below L_v=R_{max} and the mean value in brackets is calculated at a distance R_{max}/2 from the wall. Equation (9) predicts that the impact pressure on the material surface is proportional to the square of the flow velocity ($\sqrt{\Delta P}$.Dα/Dt); as the erosion rate is proportional to the square of the impact pressure, therefore it is predicted that the erosion rate would be proportional to the fourth power of the flow velocity; this finding qualitatively agrees with the experimental evidence that the erosion rate is proportional at least to the flow velocity to the fourth power; equation (9)takes into account also the effect of non-condensable gas content in the liquid by indirectly affecting the maximum bubble radius. Equation (9) also indicates that the erosion rate depends on the initial bubble size as it affects R_{max} and also on the initial bubble number density distribution as reported by Kato et al.[12].

The calculated impact pressure should be compared to the yield stress of the material considering however the cycling loading, which leads to material fatigue. Therefore an Erosion Aggressiveness Index is defined (EAI):

$$(EAI) = \frac{P_w}{\sigma_y}\log\left(\frac{\frac{L}{U}}{t_b}\right) \qquad (10)$$

where σ_y is the material yield stress, t_b the Rayleigh collapse time:

$$t_b = 0.92 \frac{R_{max}}{\sqrt{\frac{\Delta p}{\rho_l}}} \qquad (11)$$

and the *log* term considers the number of cyclic loading leading to reduced values of the yield stress due to fatigue; *U* and *L* are typical scales for flow velocity and length (i.e. for the base case, L=1mm, U=120m/s).

The advantage of the present model is that it can help in the identification of erosion zones, assuming they are caused by the collapse of a constant population of bubbles of specific initial radius R_0, pre-existing in the liquid. While it cannot take into account the possibility of bubble break-up or coalescence (i.e. bubble population change), it is a simple model that can be used for quick estimation of erosion prone regions, without needing advanced bubble tracking methods or compressible approaches for tracking pressure waves.

The Flows under Investigation

The ability of the proposed erosion aggressiveness index (EAI) as also of the (CAI) to identify regions prone to cavitation erosion is tested in two experimental test cases for which experimental or and computational data have been published. The first one is related to erosion due to cavitation inside the nozzle of a fuel injection type layout and the other refers to erosion of the needle of a commercial injector.

The flow field in an injector nozzle model.

The geometry under investigation has been studied numerically and experimentally and results have been reported for the erosion of the nozzle under various cavitating conditions and fuels, Perkovic et al. [13]. The flow configuration with its geometrical layout is shown in fig.1a; for purposes of the development of the erosion aggressiveness index, and to reduce computational time, the flow was assumed two dimensional; the operating fluid is diesel and the operating conditions are shown on table 1; the cavitation number (*CN*) as also a typical Reynolds number (*Re*) are also shown on table 1 with the fuel thermodynamic properties.

Modelling details

The transport equations governing the flow development are based on the assumptions of incompressible fluid, single fluid homogeneous mixture of liquid and vapour, steady state flow with a k-ω model of turbulence. Cavitation model is that of Sauer et al. [15] and higher order discretization schemes on all transport equations have been employed; as the state of the converged solution affects the results particularly for the vapour phase, the convergence criterion of all transport equations was set to 10^{-6}. A commercial software was employed, Fluent [15] for the numerical solution of the transport equations.

The layout of the computational domain and the numerical grid

Figure 1b shows the computational domain with the numerical grid finally employed; a telescopic grid refinement approach has been followed until a grid independent solution was achieved; finally 5 levels of grid refinement were found adequate for grid independency, giving an equivalent number of ~32 million cells inside the channel, if a uniform grid had been used at minimum employed cell length, whilst the actual number of grid nodes used was 50000; the grid cells were all almost orthogonal with maximum aspect ratio of 2. The y_+ for the near the wall surface cells was kept always in the region of 50 in compatibility with the employed wall functions.

P_{in} (bar)	P_{out} (bar)	P_v (Pa)	ρ (kg/m3)	μ (Pa.s)	*Re*	*CN*
100	40	892	828	2.14e-3	28000	1.5

Table 1: Operating conditions and liquid properties

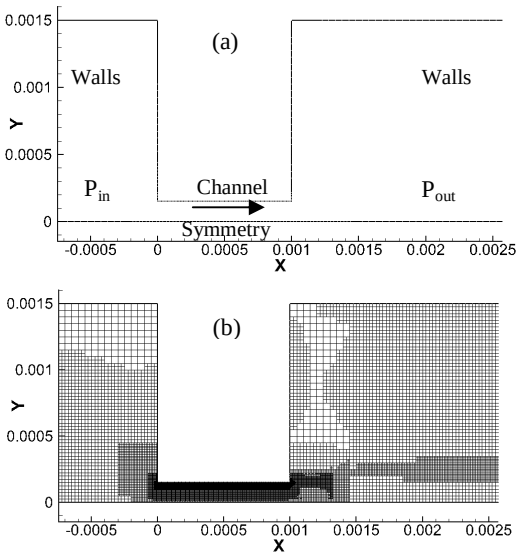

Fig.1: (a) The layout of the injector nozzle model, X-axis (y=0) is a symmetry. (b) The telescopic grid of five levels of refinement

The development of the flow field

Fig. 2 presents some flow characteristics inside the narrow channel of the injector. The high area contraction ratio at the nozzle entrance leads to considerable flow acceleration at the middle area of the channel along the central symmetry plane; also due to the 90 degrees corner at inlet, strongly reduced velocities are found with a separated region after that attached on the upper wall. The pressure levels in the separated region are the saturation pressure of the liquid and thus cavitation takes place filling the separation cavity with vapour, fig. 2c; the length of the cavity with vapour inside extends almost to the half of the length of the channel; high turbulence levels are found at the edges of the cavity due to the development of strong shear layers. The liquid volume fraction distribution in the channel is in a very good agreement with that predicted by Perkovic et al.[13] as also with the experimental results of Winklhofer et al. [18] for a very similar flow situation; the cavitation length extends up to 60% of the channel length with the effect of the re-entrant jet lifting the cavity tip off the wall. The velocity distribution at the exit of the channel has been predicted by Perkovic et al. [13] and it is shown with the present predictions in Fig. 3.

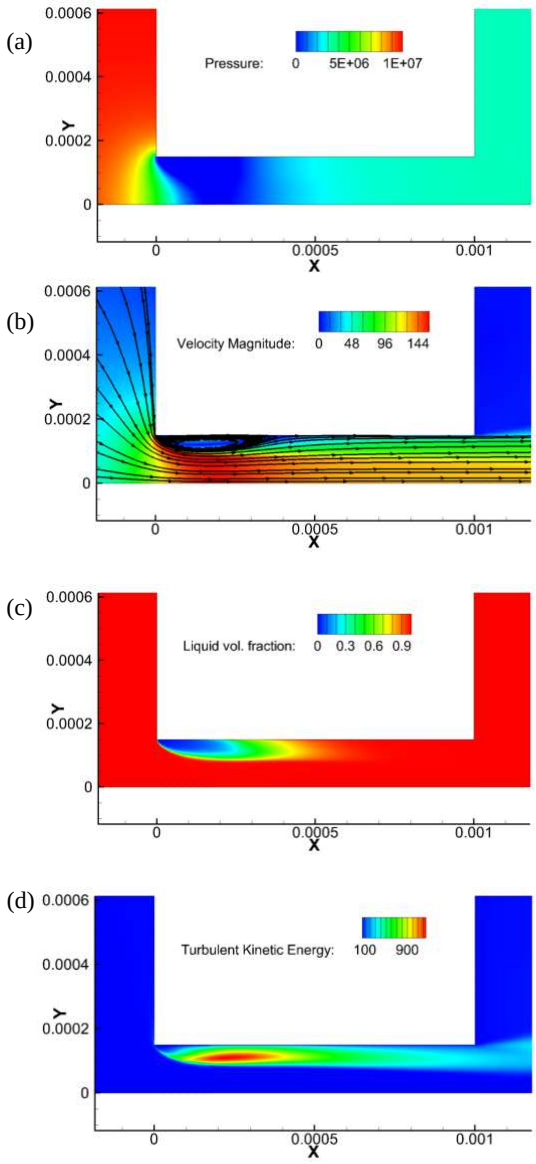

Fig. 2(a, b, c, d): The pressure, velocity magnitude, liquid volume fraction and turbulent kinetic energy inside the injector nozzle (flow from left to right)

Perkovic et al. [13] results were obtained assuming a three dimensional flow field with a coarse grid in the third direction utilizing a two phase model; the agreement between the two cases was satisfactory as near the wall the present methodology employs a very fine mesh and the three dimensionality effects which are considered in [13] explain the small differences in the central region; the predicted mass flow is 7.73g/s compared to the 7.33g/s predicted by Perkovic et al. [13], i.e. a difference of 5% due probably to 3D effects.

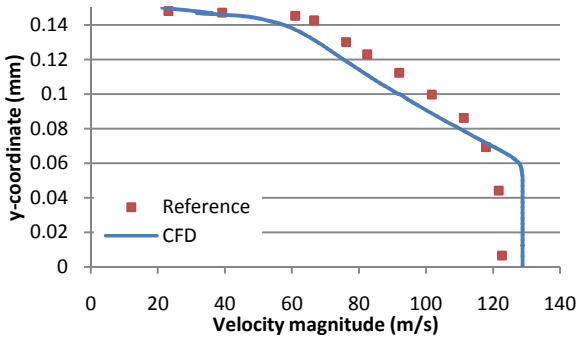

Fig.3: Velocity magnitude distribution at the channel outlet-comparison with Perkovic et al. [13]

Fig.4a shows the near wall flow velocity along the wall (at a distance of y=0.1495mm from the symmetry plane); the reverse flow region which starts right at the corner creating a very small bubble and then leading to cavity extending up to 40% of the channel length; however the vapour cavity, shown in fig. 4b, extends further downstream to 60% of the channel length in agreement with the cavity vortex sitting at the tip closure of the vapour cavity, see fig.2b.

Erosion Indexes

Figure 5a presents the distribution of the near wall total derivative of vapour volume fraction while fig. 5b shows the total derivative of pressure along the wall; according to [9] the flow region defined by equations (2) indicate the surface region prone to erosion due to hydrodynamic effect (no material properties are involved). The total derivative of pressure along the wall on the condition of negative total derivative of vapour fraction (i.e. bubble collapse) indicates wall regions prone to erosion damage due to bubble collapse; this surface region prone to bubble erosion is in agreement with the surface region predicted by [13]; however erosion progression also depends on the material properties as well, apart from the strength of bubble collapse and its frequency.

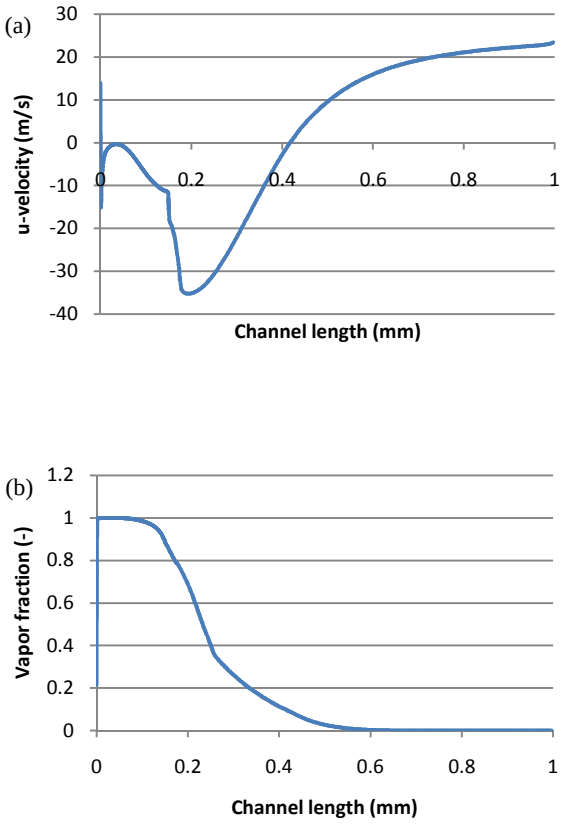

Fig. 4(a, b): (a) Near wall streamwise velocity distribution along the wall, (b) Vapour fraction distribution along the wall

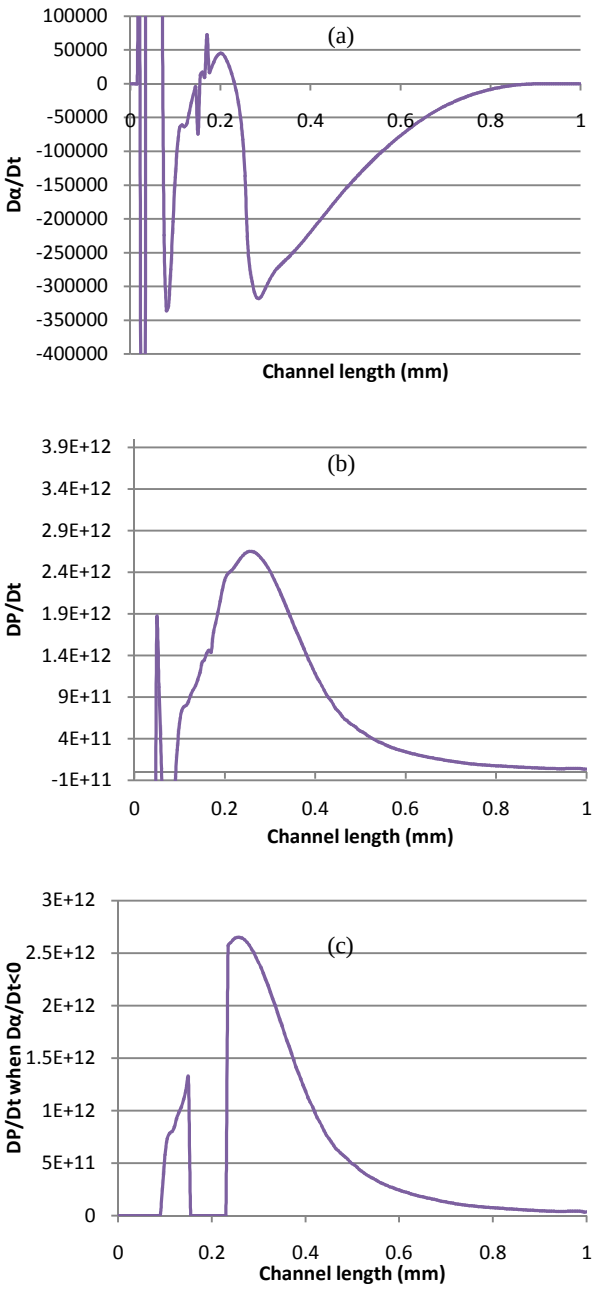

Fig. 5(a, b, c): (a)Total derivative of vapour fraction, (b) Total derivative of pressure, (c) Wall region prone to erosion damage. All calculated at a distance $L_v=R_{max}/2$, for a bubble of $R_0=4.5\mu m$

As outlined before the present work proposes an Erosion Aggressiveness Index (EAI), equation (10), which connects flow aggressiveness with material properties. Fig. 6 indicates the values of (EAI) along the channel wall (made of steel, SS316L, with $\sigma_y=400MPa$) for three initial bubble radii (R_0) at the injection pressure. On the same figure the predicted erosion results, taken from [13] are also shown.

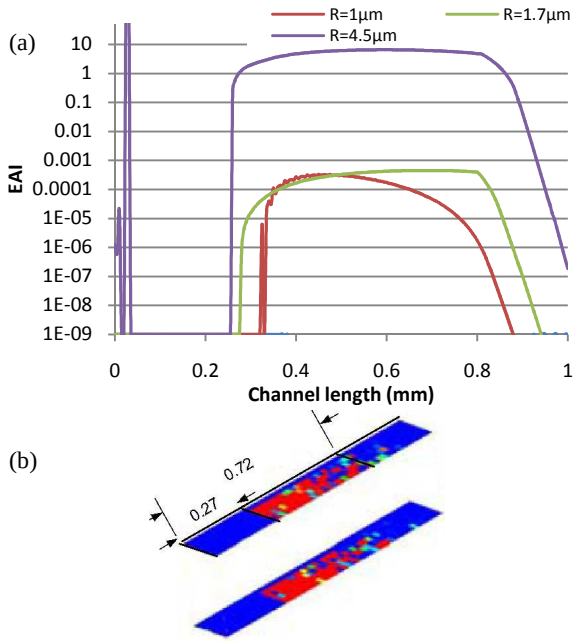

Fig. 6(a, b): (a) EAI for various initial bubble diameters. (b) Results on erosion rate from Perkovic et al. [13]

It is concluded that the collapse of bubble of initial diameters smaller than 1.7μm are not capable of contributing to erosion damage, whilst bubbles of initial diameter larger than 4.5μm have erosion effects starting early in the channel wall towards the end of the channel length; the damaging capability of the collapsing bubbles is increasing with a power of their size, with bubbles of size of 4.5μm to start their possible damaging contribution as early as 0.25mm from the channel inlet in agreement with measurements. The cumulative damage effect due to all bubbles will depend on the number density distribution of the bubbles and it is a concept unknown in most engineering cases.

Application to Diesel injectors

The aforementioned erosion model, formulated in eq. (9) and (10), has been also applied to the prediction of erosion patterns inside Diesel

injectors. In this section, the results of cavitation erosion aggressiveness on two different injectors shall be analysed.

The two injector geometries, as well operating conditions and lift law, have been provided by Caterpillar Inc. The two injectors share exactly the same needle, but differ in the sac volume size and hole tapering. Injector A has cylindrical holes, whereas injector B has slightly tapered holes; an indicative schematic is shown in Fig. 7.

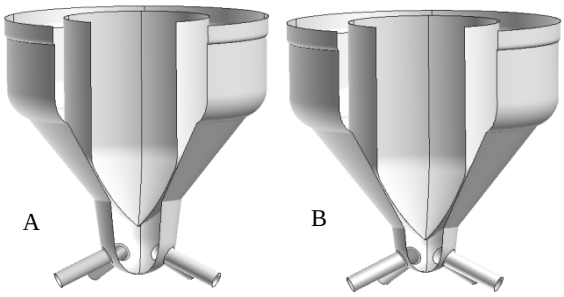

Fig. 7: The two examined injector geometries. Note the differences in sac volume.

Both injectors feature a 5-hole mini sac type nozzle, operating at a discharge pressure of ~1800bar; as mentioned above, the exact pressure pulse for each injector has been provided by Caterpillar, along with the corresponding lift law. Only a sector of 72^o ($1/5^{th}$) of the two injectors has been simulated for one injection cycle; symmetry boundary conditions are imposed on the symmetry planes. Due to the case set-up, eccentric needle motion has been omitted in this study; this is a possible source of discrepancy, since in reality it has been found that eccentric needle motion is rather significant at low lifts. Erosion has been estimated by post processing the instantaneous flow results.

The developing flow within the injectors is significantly affected by the sac volume, since the Coanda effect forces the flow to attach on the injector needle for injector A and on the wall for injector B; the interested reader is addressed to the previous work of the authors [11] for more information on the methodology and flow field results. In both injectors, cavitation nucleation occurs at two locations mainly: one is between the needle and the needle seat and the other is at the injector orifice entrance. Cavitation occurrence is higher in injector A; this is a direct consequence of hole tapering. For the estimation of erosion aggressiveness, averaging is performed at each component of the injector, for the time interval that cavitation is relevant.

Results of the erosion aggressiveness post-processing are shown below, in Fig. 8 and Fig. 9. In these cases, the initial bubble radius used was 1μm, which is consistent with the value used for the cavitation model set-up. Also in fig. 8 and 9 the X-ray images, with the actual erosion are shown.

A general observation from Fig. 8 and Fig. 9, is that in both injectors high values of the erosion aggressiveness index are found at various locations; while the predicted values are below unity, their locations seem to correlate with locations of actual erosion. Indeed, erosion has been found to develop in both injectors after performing X-ray scans after ~1000 operating hours.

Comparing the EAI between the two injectors, one can clearly see that there is a higher aggressiveness in injector A inside the sac volume, whereas in injector B there are high values towards the needle seat. The above are partly confirmed by the experimental observations, since it is found that injector A has indeed erosion occurrence inside the sac volume, however injector B has only slight signs of erosion inside the sac and nothing on the needle seat.

With respect to the needle erosion, injector B has significantly higher EAI on the needle, than injector A, almost 300% higher. This is confirmed by experimental observations, since injector A has only a slight indentation on the needle, whereas injector B has a deep engraving, after operation.

Finally, with respect to erosion in the hole region, in injector A high EAI values are found at the lower hole surface, where actual erosion develops. On the other hand, in the hole of injector B, EAI values are almost zero, which corresponds to the experiment, since injector B is practically erosion free.

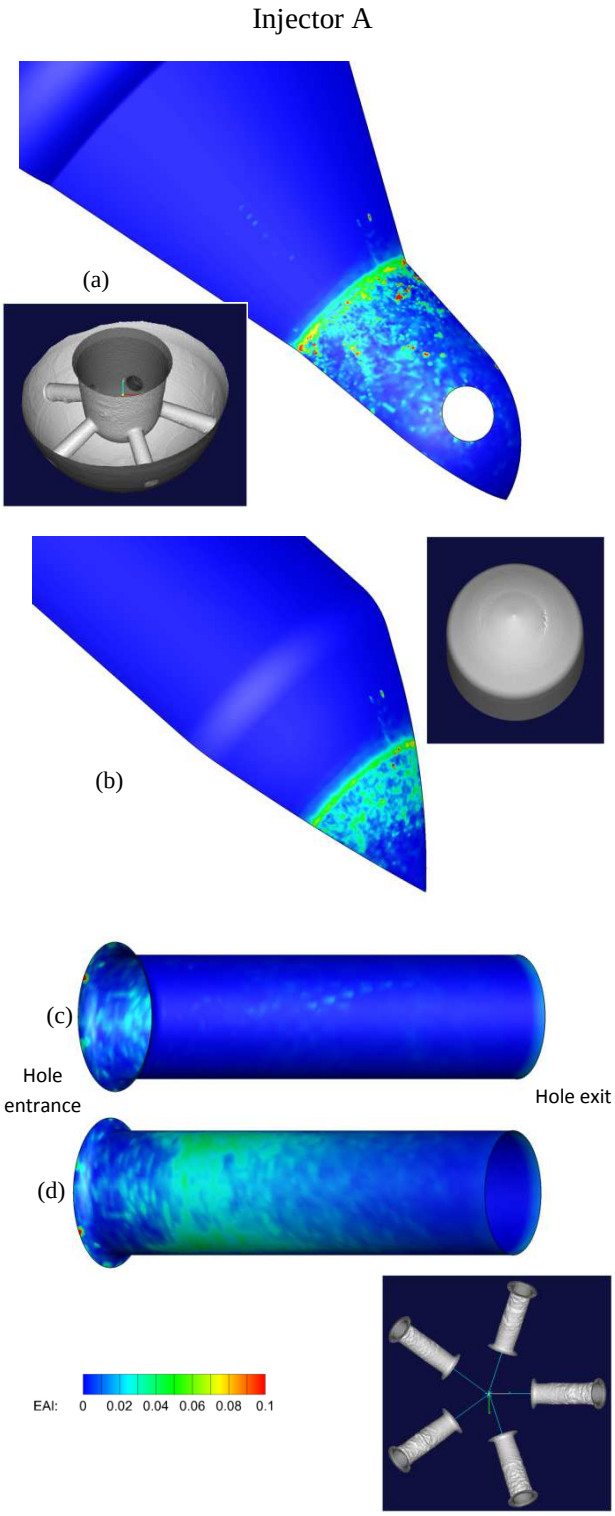

Fig. 8. Erosion Aggressiveness Index at the different injector components: (a) body, (b) needle, (c) upper, (d) lower hole surface. Not in scale.

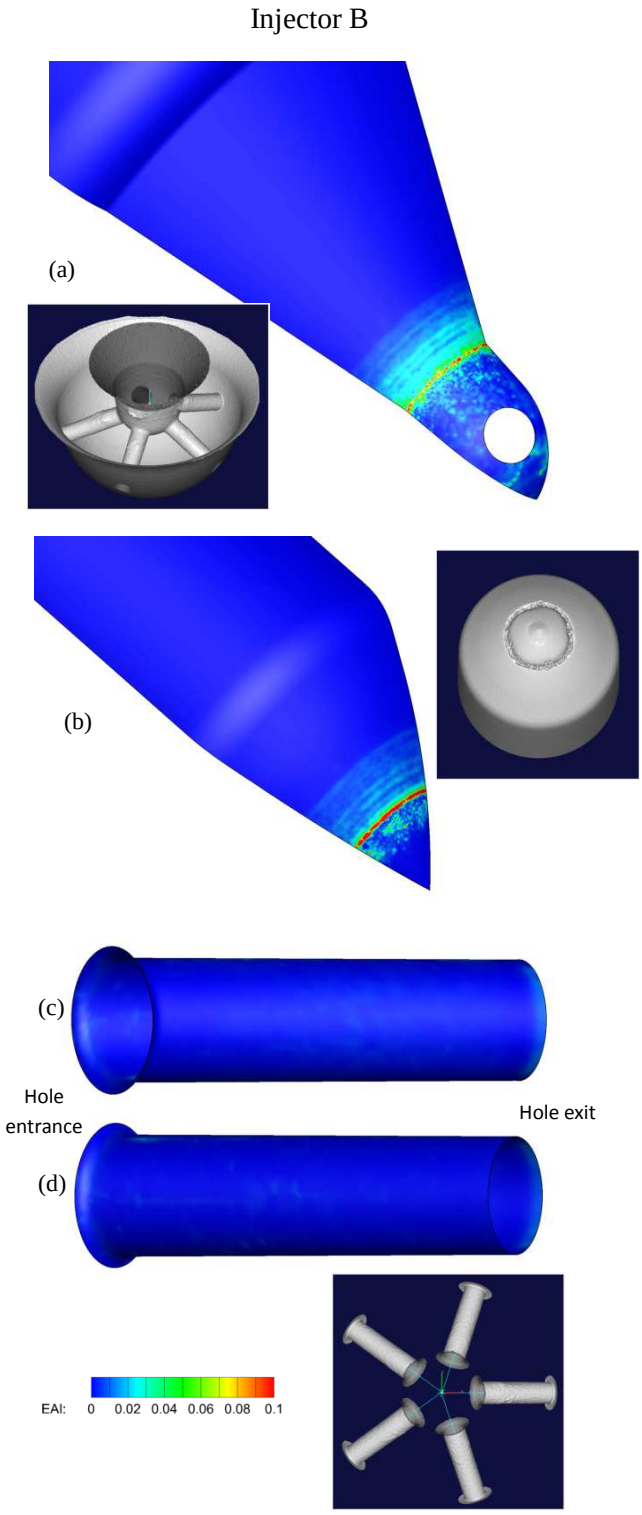

Fig. 9. Erosion Aggressiveness Index at the different injector components: (a) body, (b) needle, (c) upper, (d) lower hole surface. Not in scale.

From experiments, the location of maximum erosion is found at the lower surface of the hole of A injector and at the needle of B injector, in the form of a ring (see also Fig. 8 and Fig. 9). The described methodology is able to capture the higher intensity of erosion at the needle and the lower surface of the injector A hole, but generally under predicts the actual EAI values. This could be possibly related to the selected bubble size and bubble distribution.

Conclusions

The main conclusions of the present investigation are: in Complex engineering flows cavitation is qualitatively and fairly quantitatively well predicted; the proposed analytic expression for the impact pressure on material surfaces due to bubble collapse differentiates the erosive effect of collapsing bubbles depending on their size; the proposed Erosion Aggressiveness Index (EAI), based on the RANS equations, correlates well with published data, thus offering to the engineering community a predictive tool for the surface areas to be eroded due to bubble collapse.

References

1. Brennen C. E., Cavitation and Bubble Dynamics, Oxford University Press, 1995.
2. Franc J.P. and Michel J. M. (eds), Fundamentals of Cavitation, Kluwer, 2004.
3. Iwai Y., Okada T. and Tanaka S., A Study of cavitation bubble collapse pressure and erosion, part2: Estimation of erosion from the distribution of bubble collapse pressures, Wear 133 (1989) 233-243.
4. Fortes-Patella R., Challier G., Reboud Jl., Archer A., Cavitation erosion mechanism: Numerical simulations of the interaction between pressure waves and solid boundaries, CAV 2001.
5. Dular M., Stoffel B., Sirok B., Development of a cavitation erosion, WEAR 261 (2006) 642-655,doi: 10.1016/J.2006.01.020
6. Plesset N.S., Chapman R.B., Collapse of an initially spherical vapour cavity in the neighbourhood of a solid boundary, JFM 47 (1971) 283-319.
7. Dular M., Coutier-Delgosha O., Numerical Modelling of cavitation Erosion, Int. J. of Numerical Methods in Fluids, 2009; 61: 1368-1410, DOI; 10.1002/FLD.2003.
8. Ziru Li, Assessment of cavitation erosion with a multiphase RANS, PhD Delft Univ., 2012.
9. Bergeles G., Koukouvinis P., Gavaises M., A cavitation Aggressiveness Index (CAI) within the RANS methodology for cavitating Flows, Proceedings of the 11th International Conference on Hydrodynamics (ICHD 2014)October 19 – 24, 2014, Singapore
10. Franc, J. P., Incubation Time and Cavitation Erosion Rate of Work-Hardening Materials, Journal of Fluids Engineering, 2009, Vol. 131(2):021303-1
11. Koukouvinis P. K., Bergeles G., Li J. Z., Wang L., Theodorakakos A., Gavaises M., Simulation of cavitation inside diesel injectors, including erosion modelling, Proceedings, I. Mech. Eng., London, 10-11 March 2015.
12. Kato H., Konno A., Maeda M., Yamaguchi H., Possibility of Quantitative Prediction of Cavitation Erosion Without Model Test, Transactions of ASME, Fluids Engineering, Vol. 118, Sept 1996, pp 582-588.
13. Perkovic, L., Greif D., Taschl R., Priesching P., Duic N., 3D CFD Calculation of Injector Nozzle Model Flow for Standard and Alternative Fuels, HEAT 2008, Fifth International Conference on Transport Phenomena In Multiphase Systems, June 30-July 3, 2008, Bialystock, Poland.
14. Hattori S., Hirose T., Sugiyama, Prediction Method for Cavitation Erosion Based on Measurements of Bubble Collapse Impact Loads, 6th Int. Symp. On Measurement Techniques for Multiphase Flows, Journal of Physics, Conference series 147 (2009) 012011, doi: 10.1088/1742-6596/147/1/012011
15. ANSYS Fluent 14.5.7 manual.
16. Skoda R., Iben U., Morozov A., Mihatsch M., Schmidt S., Adams N., Numerical Simulation of Collapse Induced Shock Dynamics for the Prediction of the Geometry, Pressure and temperature Impact on the Cavitation Erosion in Micro Channels, IMRC 3rd International Cavitation Forum 2011, 2011

17. Edelbauer W., Morozov A., Strucl J., Large Eddy Simulation of Cavity Throttle Flow, Simhydro 2014 on Modelling of Rapid Transitory Flows.
18. Winklhofer E., Kull E. ,Kelz E. ,Morozov A., Field Documentation in Model Throttle Experiments Under Cavitation Conditions, ILASS-Europe 2001, Zurich.

Nomenclature

α: Vapour volume fraction
ΔP: pressure difference (=P_l-P_v) (Pa)
μ: liquid viscosity
ρ_l: liquid density (kg/m^3)
σ: Surface tension (N.m^{-1})
σ_y: material yield stress (Pa)
φ: surface inclination of the wall to the radius connecting the bubble center and the center of the wall surface element.
CN: Cavitation number ($CN = \frac{P_{in}-P_{out}}{P_{out}-P_v}$)
Dα/Dt: total derivative of vapour volume fraction (s^{-1})
DP/Dt: Total derivative of pressure (Pa.s^{-1})
L: typical macroscopic length scale of the flow (m)
L_v: region of influence of collapsing bubbles (m)
n_0: number of bubbles per unit volume (m^{-3})
P_{ac}: emitted pressure pulse (Pa)
P: Pressure (Pa)
P_{g0}: Gas pressure inside the bubble of radius R_0(Pa)
$P_{w,imp}$: Impulse pressure (Pa.s)
P_w: pressure load on the wall (Pa)
P_l: liquid Pressure at bubble 'infinity' (Pa)
P_v: Liquid saturation pressure (Pa)
*r:*bubble distance from the wall (m)
R: Local bubble radius (m)
R_0: Initial bubble radius (m)
$\dot{R}$: Bubble wall velocity (m/s)
R_{max}: maximum bubble radius (m)
t: time (s)
t_b: Bubble collapsing time
$t_b = 0.92 \frac{R_{max}}{\sqrt{\frac{\Delta p}{\rho_l}}}$ (s)
V_{vol}: volume of integration

Contact information

Professor M. Gavaises

Department of Engineering and Mathematical Sciences, City University, Northampton Square, London, EC1V0HB, UK

Email: M.Gavaises@city.ac.uk

Acknowledgments

The research leading to these results has received funding from the People Programme (Marie Curie Actions) of the European Union's Seventh Framework Programme FP7/2007-2013/ under REA grant agreement n. 324313.